SIAM J. Applied Dynamical Systems
Vol. 13, No. 2, pp. 944–957

An Energy-Optimal Methodology for Synchronization of Excitable Media*

Dan Wilson† and Jeff Moehlis†

Abstract. We propose a novel energy-optimal methodology to synchronize the cells within an excitable medium during spiral wave activity. The optimal stimulus takes the cells of an excitable medium to a target set where the isostables of the system, which measure the time it takes for a given initial condition in phase space to approach a stable fixed point, are diffuse, thereby synchronizing the activity of the medium. This method is illustrated for a FitzHugh–Nagumo-based model which captures important characteristics of the myocardium and represents a significant first step in the development of energy-optimal defibrillation strategies.

Key words. excitable media, synchronization, Hamilton–Jacobi–Bellman, optimal control, isostables

AMS subject classifications. 49J15, 92B25, 35Q92, 34K17

DOI. 10.1137/130942851

1. Introduction.

Spiral waves and spatiotemporal chaos are commonly seen in excitable media such as the Belousov–Zhabotinsky reaction and in the electrochemical activity of both the retina and the heart muscle [41]. In the heart, spiral waves are associated with cardiac arrhythmias and can lead to serious health consequences. Ventricular fibrillation, for example, is caused by the presence of unwanted spiral waves within the myocardium which interfere with normal sinoatrial rhythm and can be deadly within minutes [14], [7], [2]. Such considerations have motivated the research community to propose ways to terminate spatiotemporal chaos in excitable media, typically by annihilating spiral wave cores (also known as rotors). For example, the method from [36] gives a control strategy to absorb spiral waves by stimulating the excitable medium on a grid of control points. Reference [42] explores the possibility of suppressing spiral waves by generating target waves at a point source within the excitable medium. More recently, [8], [21], [23], and [16] have found that a pulsed electric field progressively synchronizes the cells in the myocardium and successfully terminates spiral wave activity using lower shock intensity through the formation of virtual electrodes associated with heterogeneities in the medium.

The mechanisms of defibrillation are not fully understood, but one prevalent theory is that defibrillation restores normal functioning of the heart by not only terminating spiral wave activity, but also by sufficiently synchronizing myocardial activity to prevent reentry of new spiral waves [4], [5], [37], [13]. Temporary termination of spiral wave activity can be accomplished by simply activating quiescent cells in the excitable medium, but reentry is much more difficult to prevent. For this reason, in this paper we focus on a novel and energy-efficient method for synchronization of cells within an excitable medium.

*Received by the editors October 25, 2013; accepted for publication (in revised form) by D. Barkley March 25, 2014; published electronically June 3, 2014.
http://www.siam.org/journals/siads/13-2/94285.html
†Mechanical Engineering Department, University of California at Santa Barbara, Santa Barbara, CA 93106 (dan.d.wilson8@gmail.com, moehlis@engineering.ucsb.edu).

We devise a natural framework that characterizes the synchronization of excitable tissue using the notion of isostables [25], which measure the time it takes for a given initial condition in phase space to approach a stable fixed point. Cells which start on the same isostable will approach the fixed point synchronously, regardless of their initial distance from each other in phase space. Using this framework, we illustrate a general procedure for finding an energy-optimal stimulus for driving the states of each cell to a region of phase space where isostables are diffuse, thereby synchronizing the activity of the cells. This methodology is novel in that it uses the isostables of the excitable system [25] (an analogue of isochrons for asymptotically periodic systems) to choose a target set which will greatly synchronize cell activity even if the system is not fully controllable. We emphasize that this work is not meant to be a methodical study of defibrillation techniques, but rather a significant first step toward the development of novel defibrillation strategies.

In section 2 we introduce our model and discuss the dynamics that are relevant to the presence of spiral waves in excitable media. Section 3 gives a discussion of isostables and their importance in forming a useful control objective. In section 4 we formulate an optimal control problem using a Hamilton–Jacobi–Bellman approach. Section 5 gives the results of our optimal control problem as well as simulations using the optimal control strategy. Concluding remarks are given in section 6.

2. Model.

The FitzHugh–Nagumo equations have been proposed as a model of the myocardium which captures important characteristics of excitable media but is still simple enough to allow for detailed analysis [34] (cf. [9], [1]):

$$\begin{aligned} \dot{V} &= \nabla(D\nabla V) + f_V(V,w) + u(t), \\ \dot{w} &= f_w(V,w), \end{aligned} \tag{1}$$

with zero-flux, Neumann boundary conditions (i.e., $(\nabla V)\cdot \mathbf{n} = 0$, where $\mathbf{n}$ is a vector normal to the boundary). Here,

$$\begin{aligned} f_V(V,w) &= c_1 V(V-a)(1-V) - c_2 V w, \\ f_w(V,w) &= b(V - dw). \end{aligned}$$

The diffusion tensor, D, is taken to be a matrix with 1×10^{-3} on the diagonal and zero elsewhere, corresponding to isotropic tissue. Nondimensionalized variables V and w represent membrane voltage and gating variables, respectively, $u(t)$ is the common control input, $b = 0.013$, $c_1 = 0.26$, $c_2 = 0.1$, and $d = 1$. We will simulate (1) on a uniform, 256×256 grid with cell spacing $dx = dy = 0.1$. We take each grid point to be an individual, noisy cardiomyocyte. With a second order spatial discretization of (1), it follows that

$$\begin{aligned} \dot{V}_{i,j} &= 0.2\,(V_{i-1,j} + V_{i+1,j} + V_{i,j-1} + V_{i,j+1} - 4V_{i,j}) + f_V(V_{i,j}, w_{i,j}) + \eta_{i,j}(t) + u(t), \\ \dot{w}_{i,j} &= f_w(V_{i,j}, w_{i,j}). \end{aligned} \tag{2}$$

Here, $i,\ j = 1,\ \ldots,\ N$ are the spatial positions of each cell in a two-dimensional representation of the myocardium, and $\eta_{i,j}(t) = \sqrt{2K}\mathcal{N}(0,1)$ is the independent and identically distributed noise associated with each cell, assumed to be zero-mean Gaussian white noise

with variance $2K$. For simulations with noise, we take $K = 5 \times 10^{-5}$. We note that simulation results do not qualitatively change as we refine the grid. Furthermore, we emphasize that while adding a uniform electric stimulus, $u(t)$, to each cell does not perfectly represent the way external defibrillation shocks depolarize the myocardium with virtual electrodes [23], it provides a starting point for developing our optimal methodology.

In the absence of noise, coupling, and control, each cell in (2) has a stable fixed point at $(V, w) = (0, 0)$ with the slower direction of the stable manifold approaching along the w-axis. Near the origin, the cell is excitable, meaning for a large enough perturbation in the positive V direction, the cell dynamics will leave the neighborhood of the origin and follow a transient attractor [15], [32] until asymptotically approaching the origin along the slow manifold (Figure 1).

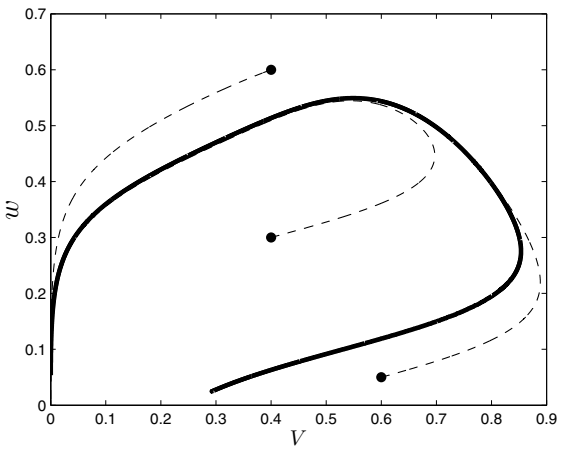

Figure 1. *The transient attractor, shown as a bold line, for a single cell from (2) without control or noise. Trajectories starting near the transient attractor will approach the stable fixed point along the transient attractor.*

In order to formulate a useful control problem, we need to understand how the cells in the model behave under the influence of spiral wave dynamics. We simulate (2) using an alternating diagonally implicit method [30] on a 256×256 grid. Figure 2 shows the time evolution of a system with multiple spiral waves, along with the states of 121 cells chosen to provide a uniform sampling over the grid. We find that throughout the simulation, the state of each cell stays reasonably close to the transient attractor.

3. Using isostables to define a control objective. Ultimately, our goal is to design a stimulus that synchronizes cell activity in our model in order to inhibit spiral wave reentry. A naive approach to solving this problem would be to find a stimulus that takes each cell in (2) to the same location in phase space. However, a less restrictive but equally effective control objective can be formulated by understanding the individual cell dynamics from the perspective of isostables.

The notion of isostables for excitable systems is analogous to the idea of isochrons for asymptotically periodic systems. For systems with stable limit cycles, isochrons extend the

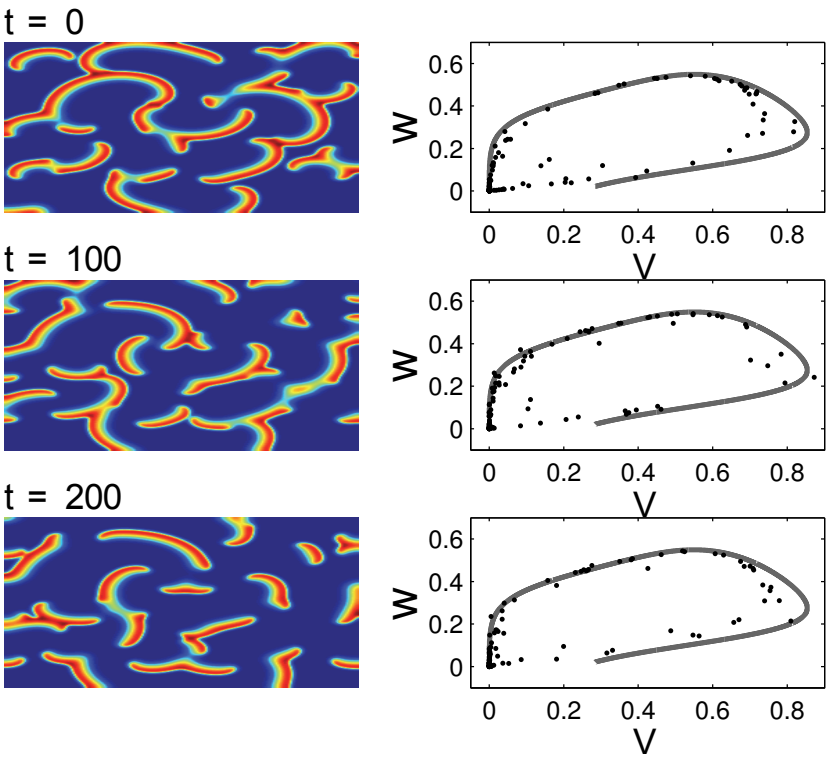

Figure 2. *Spiral waves in a network of cells described by (2). The state of each cell stays reasonably close to the transient attractor while there are spiral waves in the medium.*

notion of the phase of the oscillation to the basin of attraction of the limit cycle [41]. However, it is not possible to define a phase for an excitable system because there is no periodic orbit. Instead, we use isostables to find points in phase space that approach the fixed point in the same way. As detailed in [25], given a system with a stable fixed point with real eigenvalues and a system observable $f(\mathbf{x})$, we define the quantity

$$\mathcal{I}(\mathbf{x}) = \lim_{T\to\infty} \frac{1}{T} \int_0^T (f \circ \phi(t, \mathbf{x})) \exp(-\lambda t) dt, \tag{3}$$

where $\phi(t, \mathbf{x})$ is the evolution of the state over time, and λ is the magnitude of the largest (least negative) eigenvalue for the system linearized around the fixed point. Using (3), we can define isostables as the level sets of $\mathcal{I}(\mathbf{x})$. Isostables are useful in this context because two initial points lying on the same isostable, no matter how far apart, will approach the fixed point synchronously. Thus, in order to synchronize the activity of the medium, we do not strictly need to drive the state of each cell to the same location in phase space. Instead, we need only to drive the state of each cell to the same isostable, or at least to isostables with values that are close together.

Using this approach, we define our system observable for a single cell from (2) in the absence of noise, coupling, and control as $f(\mathbf{x}) = V + w$, and systematically calculate different

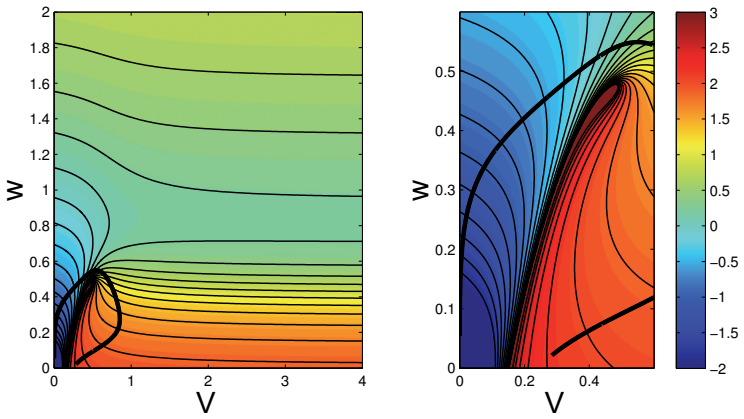

Figure 3. *The quantity* $\log(\mathcal{I}(\mathbf{x}))$ *is shown in color for* (2)*. The color map shown on the right will be used throughout this work. Isostables which are equally spaced in time are also shown. The plot on the right shows an enlarged view near the transient attractor. The isostables are relatively diffuse for* $(V, w) \approx (1.2, 0.8)$*.*

values of $\mathcal{I}(\mathbf{x})$ for different grid points. Figure 3 shows a plot of $\log(\mathcal{I}(\mathbf{x}))$. The logarithm is taken so that each isostable is equally spaced in time, and the transient attractor is plotted as a thick black line for reference.

Viewing the problem of myocardial synchronization through the lens of isostables provides a quantitative framework that allows us to formulate an optimal control problem which may not be intuitive from merely observing the phase space. For instance, the top-left panel of Figure 4 shows three different cells with different initial conditions along the same isostable. Each produces differently shaped action potentials (top-right panel), but the cells become quiescent at the same time. Conversely, the bottom-left panel of Figure 4 shows three cells with the same initial transmembrane voltage, but on different isostables. The bottom-right panel shows that each cell becomes quiescent at different times.

From Figure 3 it is apparent that the isostables become particularly diffuse for $(V, w) \approx (1.2, 0.8)$. Thus, if we attempt to drive each of the cells to an isostable in this region, but miss the target slightly, the deviation as measured by the isostables will be smaller than if we missed the target in a region where the isostables are more densely packed. This gives a novel control strategy for synchronizing the activity of the medium: drive the system to a region of phase space for which the isostables are diffuse.

4. Optimal control.

We consider a system of two identical, deterministic, uncoupled cells with a control signal $u(t)$ applied to both cells:

$$\dot{z} = F(z) + Bu(t), \tag{4}$$

where $z = \begin{bmatrix} V_1 & w_1 & V_2 & w_2 \end{bmatrix}^T$, $B = \begin{bmatrix} 1 & 0 & 1 & 0 \end{bmatrix}^T$, and

$$F(z) = \begin{bmatrix} f_V(V_1, w_1) \\ f_w(V_1, w_1) \\ f_V(V_2, w_2) \\ f_w(V_2, w_2) \end{bmatrix}. \tag{5}$$

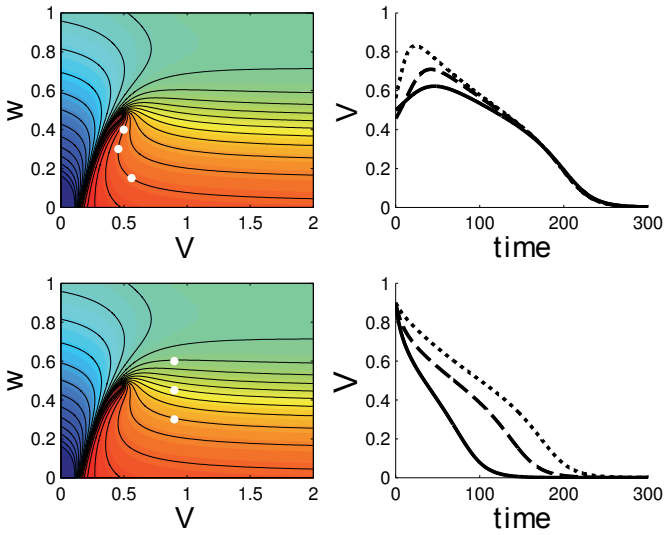

Figure 4. *Left panels show the initial states of three different cells along the same isostable (top-left panel) and same initial voltages (bottom left panel). The right panels show the associated action potentials for each cell.*

The control objective is to find an optimal control law that will take the system to the same isostable (see section 3) so that each cell approaches the transient attractor in the same way, thereby synchronizing the activity of the medium. We solve this problem using a Hamilton–Jacobi–Bellman (HJB) approach [17], [27]. In most cases, the HJB equation cannot be solved exactly. Furthermore, for a numerical solution, the amount of computations required and memory needed to store the solution grows exponentially with the dimensionality of the problem. Ideally, we would like to include as many cells as possible to optimally drive to the target set, but we are limited to two, since a four-dimensional problem is already challenging given limited computing power. Furthermore, we realize that the system may not be fully controllable with only one control input; therefore we choose our target set to be the region of phase space where the isostables are diffuse, so that if we cannot control each cell exactly to the same isostable, the difference in isostables will be relatively small. For a given initial state, z, the energy-optimal stimulus will minimize

$$J(z, u(t)) = \int_0^{T_{end}} u^2 dt + \gamma q(z(T_{end})), \tag{6}$$

where $\int_0^{T_{end}} u^2 dt$ represents the amount of power consumed by the stimulus, $q(z(T_{end}))$ is an endpoint cost function, and γ is a penalizing scalar which determines the relative importance of the terms. We also consider bounds on the maximum input for practical hardware limitations and tissue sensitivity: $|u(t)| \leq u_{max}$. We define the value function (also known as the cost-to go function)

$$\mathcal{V}(z, \tau) = \min_{\substack{|u(t)| \leq u_{max} \\ \forall t \in [\tau, T_{end}]}} J \tag{7}$$

and can find the optimal stimulus for (6) by solving the HJB equation [17]

$$0 = \frac{\partial \mathcal{V}}{\partial t}(z,\tau) + \min_{|u(t)|\leq u_{max}} \mathcal{H}(z, \nabla\mathcal{V}, u), \tag{8}$$

with

$$\mathcal{H}(z, \nabla\mathcal{V}, u) = u^2 + \left[\nabla\mathcal{V}(z(t),t)\right]^T \left(F(z(t)) + Bu(t)\right), \tag{9}$$

and endpoint boundary condition

$$\mathcal{V}(z(t_{end}), T_{end}) = \gamma q(z(t_{end})), \tag{10}$$

where $\nabla\mathcal{V}$ is the gradient of the value function with respect to the state z. To find the optimal control, $u^*(t)$, we must minimize the Hamiltonian by taking the derivative of (9) with respect to u equal to zero. This result is valid, provided that the required control does not saturate, i.e., $|u^*(t)| < u_{max}$. If $|u^*(t)| \geq u_{max}$, the optimal control saturates in agreement with Pontryagin's minimum principle [29], [17]. Using (9), $\frac{\partial \mathcal{H}}{\partial u} = 2u + \nabla\mathcal{V}^T B$, and by noticing that $\nabla\mathcal{V}^T B = \mathcal{V}_{V_1} + \mathcal{V}_{V_2}$, we find

$$\begin{aligned} u^*(t) &= -\frac{1}{2}(\mathcal{V}_{V_1} + \mathcal{V}_{V_2}), && |\mathcal{V}_{V_1} + \mathcal{V}_{V_2}| < 2u_{max}, \\ u^*(t) &= -\text{sign}(\mathcal{V}_{V_1} + \mathcal{V}_{V_2})u_{max}, && |\mathcal{V}_{V_1} + \mathcal{V}_{V_2}| \geq 2u_{max}. \end{aligned} \tag{11}$$

With knowledge of the optimal control, we can simplify the Hamiltonian (9) as

$$\begin{aligned} \mathcal{H} &= \nabla\mathcal{V}^T F(z) - \frac{1}{4}(\mathcal{V}_{V_1} + \mathcal{V}_{V_2})^2, && |\mathcal{V}_{V_1} + \mathcal{V}_{V_2}| < 2u_{max}, \\ \mathcal{H} &= u_{max}^2 + \nabla\mathcal{V}^T F(z) - |\mathcal{V}_{V_1} + \mathcal{V}_{V_2}|u_{max}, && |\mathcal{V}_{V_1} + \mathcal{V}_{V_2}| \geq 2u_{max}. \end{aligned} \tag{12}$$

To calculate the optimal control $u^*(t)$ from (11), we must first solve (8) for $\mathcal{V}(z,t)$ with endpoint boundary condition (10) and Hamiltonian (9). In order to determine an appropriate endpoint condition, recall that isostables of (2) are diffuse to the right of the transient attractor in the neighborhood of $w = 0.8$. For this reason we choose an isostable in this region as the target set and fit a third order polynomial

$$w_T(V) = 0.0089V^3 - 0.0697V^2 + 0.1935V + 0.5807, \qquad V \geq 1, \tag{13}$$

and use it to formulate the endpoint cost,

$$q(z(t_{end})) = \mathcal{C}(V_1, w_1) + \mathcal{C}(V_2, w_2), \tag{14}$$

where

$$\mathcal{C}(V,w) = \begin{cases} \max\left(e^{-\left(\frac{w_T(V)-w}{\sigma_y}\right)^2}, e^{-\left(\frac{V-1}{\sigma_x}\right)^2}\right), & V \leq 1, \\ e^{-\left(\frac{w_T(V)-w}{\sigma_y}\right)^2}, & V > 1. \end{cases}$$

We use Ian Mitchell's "Toolbox of Level Set Methods" [26] in order to obtain a high accuracy, convergent approximate solution to the PDE (8) with boundary condition (10) and Hamiltonian (12). We choose $\gamma = 500$, $\sigma_x = 0.005$, $\sigma_y = 0.1$, $u_{max} = 0.3$, and $T_{end} = 65$ as simulation parameters. We note that we do not expect the system to be fully controllable to the target set and use a relatively large value for σ_y to compensate.

5. Results and discussion. We solve (8) for $\mathcal{V}(z,t)$ and use it to approximate $\mathcal{V}_{V_1}(z,t)$ and $\mathcal{V}_{V_2}(z,t)$. Using this data, we solve for the optimal control using five sets of initial conditions for cells starting on the transient attractor. Note that the initial conditions are spread out on the transient attractor to capture the natural spread in the states when spiral waves are present, as illustrated in Figure 2. Results are shown in Figure 5. As expected, we cannot always drive the system to the transient attractor in the prescribed time span. We note that the optimal control does not always distribute the vertical distance from the transient attractor equally between cells, as it is ocassionally less costly to attribute unequal shares of the endpoint cost to each cell.

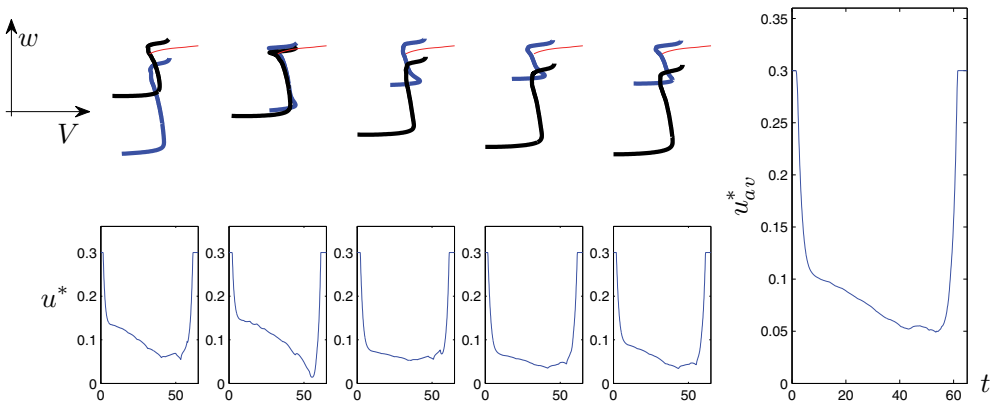

Figure 5. *Top panels give the optimal path of two different cells (plotted as thick lines) with initial conditions along the transient attractor under the influence of the computed optimal control (shown in the bottom panels). The target set is shown for reference as a thin red line. The far right panel shows the average of the* 5 *optimal stimuli,* u^*_{av}*. Note that each computed optimal stimulus exhibits similar qualitative characteristics.*

As mentioned previously, ideally we would like to determine the optimal control for not just two cells, but for as many cells as possible. However, the cost of computation grows exponentially as we increase the number of cells in the optimization. Furthermore, we notice that the qualitative characteristics of the optimal control are similar for each initial condition shown in Figure 5. For this reason, we believe that the improvement in the resulting optimal stimulus would be marginal for each cell added to the optimization. Instead, we average the five control signals from Figure 5 to determine an average optimal stimulus, u^*_{av}, shown in Figure 5. Figure 6 (see also the accompanying animation (94285_01.avi [local/web 10.1MB])) shows the time evolution for ten deterministic, uncoupled cells, equally spaced along the transient attractor and initially under the influence of the average optimal stimulus. We find that the optimal stimulus uses 1.02 units of energy and distributes the cells so that their standard deviation in $\log(\mathcal{I}(x))$ is 0.044.

Finally, inspired by works such as [8], [21], [23], and [16], we simulate (2) with spiral waves present, using three different control inputs shown in Figure 7 in order to compare their effectiveness in synchronizing the cells in the medium. In order to make meaningful comparisons with the optimal stimulus, we require both the total energy usage and total time of the pulsed

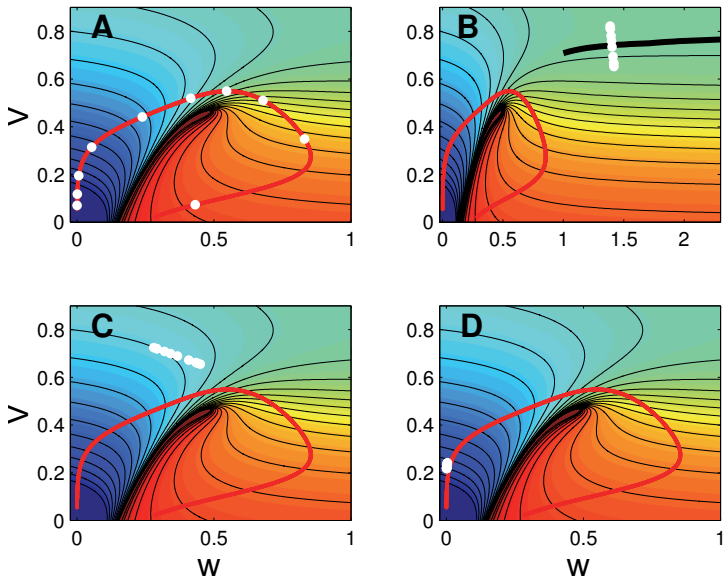

Figure 6. *Time evolution of ten cells initially distributed along the transient attractor under the action of the average optimal stimulus. Panels* A, B, C, *and* D *show the state of each cell at* $t = 0$, 65, 100, *and* 200, *respectively. See also the accompanying animation* (94285_01.avi [local/web 10.1MB]).

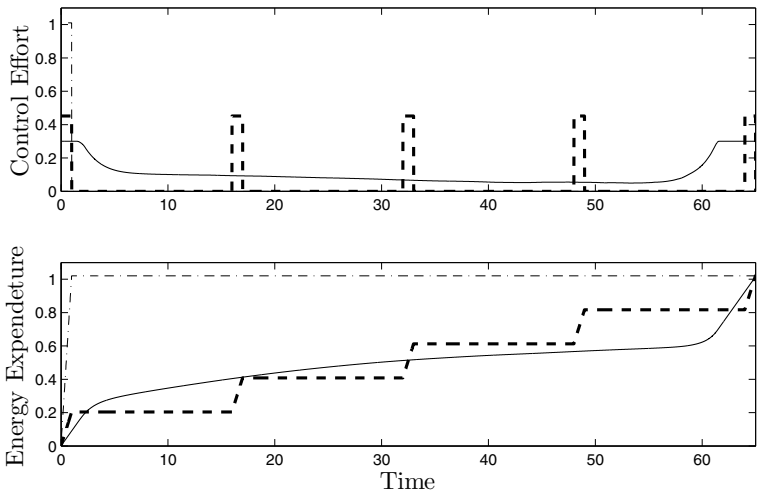

Figure 7. *The top panel shows three different control efforts. The optimal control is shown as a solid line, the multipulsed control is shown as a dashed line, and the single-pulse control is shown as a dot-dashed line. The cumulative energy expenditure is shown in the bottom panel.*

control strategy and optimal control to be equal. One such pulsed stimulus that satisfies these requirements is a square wave of one time unit duration with $u = 0.452$ applied every 16 time units, for a total of 5 pulses. Intuitively, we expect that for the pulsed strategy, the cells will

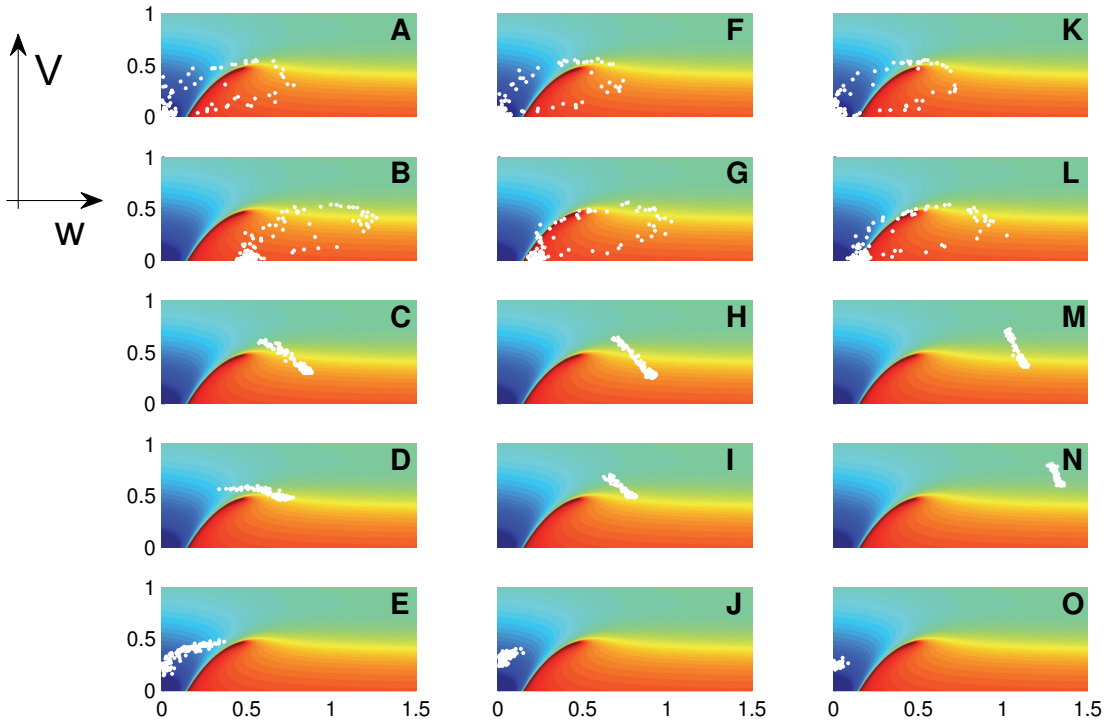

Figure 8. *Comparison of the cell synchronization for three different control strategies from Figure 7. Panels* (A)–(E), (F)–(J), *and* (K)–(O) *show the time evolution of cells for the single-pulse, multipulse, and energy-optimal strategies, respectively. From top to bottom, the rows give snapshots at* $t = -50$, 1, 32, 65, *and* 200 *with* $t = 0$ *corresponding to the moment the external control is first applied. We find that the optimal control strategy outperforms the other two strategies in terms of synchronization as measured by the final isostable distribution.*

begin to cluster near the top of the transient attractor and will become more synchronized than for the single pulse case. We have also found numerically that adding extra pulses does not have a significant effect on the overall synchronization of the cells. Furthermore, as detailed in [23], the efficacy of the pulsed strategy in preventing spiral wave reentry is related to the pulsing frequency as compared to the natural spiral frequency. However, here we are only concerned with the overall synchronization of the medium.

Results are shown in Figure 8, with panels (A)–(E), (F)–(J), and (K)–(O) showing the time evolution of cells for the single-pulse, multipulse, and energy-optimal strategies, respectively. We track the states of 121 uniformly spaced cells in the medium, and after 65 seconds, the single-pulse stimulus distributes these cells so that the deviation as measured by their isostables (i.e., $\log(\mathcal{I}(x))$) is 0.44. The multipulsed control performs better than the single-pulsed strategy with a standard deviation of 0.22 as measured by the isostables. Each successive pulse prevents the refractory cells from traveling back towards the fixed point, causing the cells to cluster over time. The optimal control outperforms both stimuli with a standard deviation of 0.06 measured by the isostables. Visually, from the voltage traces in Figure 9, it is apparent that for the optimal control strategy, the noisy cells become quiescent at more similar times

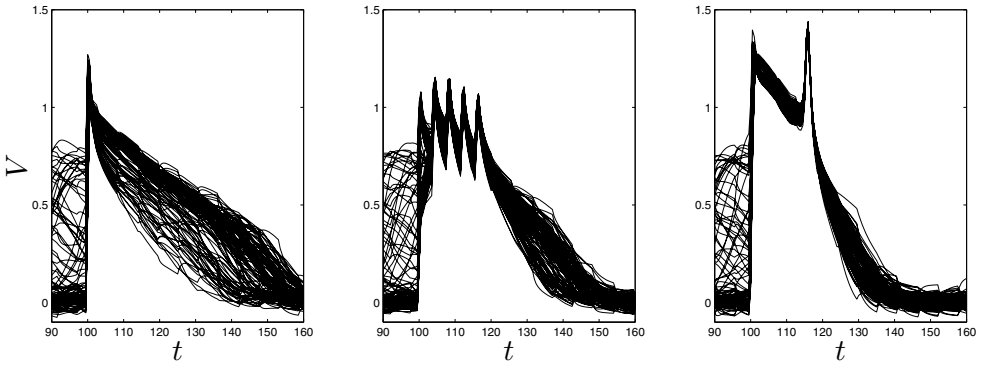

Figure 9. *Voltage traces for each cell from the simulation in Figure 8. The left, middle, and right panels show the single pulse, multipulse, and optimal control strategies, respectively. We can clearly see from the voltage traces that for the optimal control strategy, the noisy cells become quiescent at much more similar times than for the other strategies.*

than for the other strategies. For these simulations, all cells will eventually tend toward the fixed point. However, in more realistic models of cardiac defibrillation, reentry occurs when there is a distribution of quiescent and refractory cells. The cells under the influence of the optimal stimulus become quiescent at similar times, which is expected to reduce the likelihood of reentry.

6. Conclusion. This paper provides a useful mathematical framework for calculating optimal waveforms for synchronization of excitable media, illustrated here for a model of myocardial activity. This methodology is novel in that it uses isostables to predict a target set which will achieve the most synchronization among the cells. While the FitzHugh–Nagumo model is a simple representation of myocardial activity, the methodology of solving an HJB equation for the energy-optimal stimulus required to bring the cells to a region of phase space where the isostables are diffuse, thereby partially synchronizing the activity of the myocardium in order to prevent spiral wave reentry, is not model dependent.

While we have chosen a relatively simple, two-dimensional model in this work, these numerical methods can be extended to higher dimensional models, and with the expected advent of faster computing algorithms, this procedure will soon be applicable to models with more realistic ionic currents, such as [10], [38], and [24], including their generalization to bidomain models. Furthermore, the HJB formulation of the optimal control problem is fairly general and allows for the inclusion of other physiologically important considerations that may be important for defibrillation.

We acknowledge that in its current state, this method has limited experimental applicability to the problem of defibrillation. Certainly, for in vivo defibrillation, the cells within the myocardium do not receive identical stimuli, as we have assumed in (2). Also, the ultimate goal of defibrillation is to end spiral wave activity, which we have not directly addressed here. Nevertheless, this work gives the mathematical framework for development of a novel defibrillation strategy. With the ability to include more cells in the calculation by developing faster numerical algorithms, we hope to account for the spatial distribution of depolarization and

hyperpolarization caused by heterogeneities in the myocardium during defibrillating shocks. This will allow calculation of defibrillation waveforms that will be able to synchronize myocardial activity in more realistic models. Furthermore, spiral wave rotors need space to meander [7] in order to continue propagation, and synchronization could provide a mechanism for spiral wave termination by denying the rotor access to quiescent cells.

This method was applied to an excitable system with multiple spiral waves, but we note that it has potential applications for terminating cardiac alternans. Alternans is the beat-to-beat alternation of electrochemical cardiac dynamics at a constant of rate of depolarization and has been identified as a precursor to cardiac fibrillation [35]. In particular, a phenomenon known as discordant alternans, where cardiac tissue in different spatial locations exhibit alternans of action potential duration of opposite phase, can make spiral wave reentry and subsequent breakup more likely [28], [31], [40], [12]. Some previous methods to terminate alternans have focused on stabilizing the unstable period-1 rhythm [3], [33], while others have looked to terminate alternans using model-based feedback control [11]. The present method of study could be adapted to drive cells within a medium displaying discordant alternans to an isostable corresponding to the unstable, period-1 orbit as necessary, eliminating alternans without the need for continual and highly accurate monitoring of the system. This strategy may be the subject of future studies.

It is hard to overstate the importance of defibrillation in the treatment of life-threatening cardiac arrhythmias. According to the American Heart Association, there are nearly 300,000 cases of cardiac arrest each year in the United States alone [22]. Those who survive are at higher risk for further incidences of cardiac arrest and typically receive antiarrhythmic drug therapy or an implantable cardioverter defibrillator (ICD), the latter providing better long-term survival rates [19], [20]. While ICDs are an adequate long-term solution, they are far from perfect. Over time, defibrillating shocks from ICDs can lead to fibrosis in the myocardium, making it necessary to use stronger defibrillating shocks [6]. ICD shocks can also lead to adverse short-term side effects [18], [39]. We believe that the continued development of this methodology and ultimate application to defibrillation holds promise in prolonging the battery life of ICDs, which must be surgically replaced, as well as mitigating the deleterious long-term and short-term side effects of defibrillation.

REFERENCES

[1] R. R. Aliev and A. V. Panfilov, *A simple two-variable model of cardiac excitation*, Chaos Solitons & Fractals, 7 (1996), pp. 293–301.

[2] E. M. Cherry and F. H. Fenton, *Visualization of spiral and scroll waves in simulated and experimental cardiac tissue*, New J. Phys., 10 (2008), 125016.

[3] D. J. Christin, M. L. Riccio, C. A. Culianu, J. J. Fox, A. Karma, and R. F. Gilmour, Jr., *Control of electrical alternans in canine cardiac Purkinje fibers*, Phys. Rev. Lett., 96 (2006), 104101.

[4] S. M. Dillon, *Synchronized repolarization after defibrillation shocks. A possible component of the defibrillation process demonstrated by optical recordings in rabbit heart*, Circulation, 85 (1992), pp. 1865–1878.

[5] S. M. Dillon and K. Kwaku, *A unified hypothesis for defibrillation and fibrillation induction by shocks*, J. Cardiovascular Electrophysiol., 9 (1998), pp. 529–552.

[6] A. Epstein, G. Kay, V. Plumb, S. Dailey, and P. Anderson, *Gross and macroscopic pathological changes associated with nonthoracotomy implantable defibrillator leads*, Circulation, 98 (1998), pp. 1517–1524.

[7] F. Fenton, E. Cherry, H. Hastings, and S. Evans, *Multiple mechanisms of spiral wave breakup in a model of cardiac electrical activity*, Chaos, 12 (2002), pp. 852–892.
[8] F. H. Fenton, S. Luther, E. M. Cherry, N. F. Otani, V. Krinsky, A. Pumir, E. Bodenschatz, and R. F. Gilmour, *Termination of atrial fibrillation using pulsed low-energy far-field stimulation*, Circulation, 120 (2009), pp. 467–476.
[9] R. FitzHugh, *Impulses and physiological states in theoretical models of nerve membrane*, Biophys. J., 1 (1961), pp. 445–466.
[10] J. J. Fox, J. L. McHarg, and R. F. Gilmour, *Ionic mechanism of electrical alternans*, Amer. J. Physiology-Heart Circulatory Physiol., 282 (2002), pp. H516–H530.
[11] A. Garzón, R. O. Grigoriev, and F. H. Fenton, *Model-based control of cardiac alternans in Purkinje fibers*, Phys. Rev. E, 84 (2011), 041927.
[12] A. Gizzi, E. M. Cherry, R. F Gilmour, Jr., S. Luther, S. Filipp, and F. H. Fenton, *Effects of pacing site and stimulation history on alternans dynamics and the development of complex spatiotemporal patterns in cardiac tissue*, Frontiers Physiol., 4 (2013), 71.
[13] R. Gray and N. Chattipakorn, *Termination of spiral waves during cardiac fibrillation via shock induced phase resetting*, Proc. Natl. Acad. Sci USA, 102 (2005), pp. 4672–4677.
[14] R. A. Gray, A. M. Pertsov, and J. Jalife, *Spatial and temporal organization during cardiac fibrillation*, Nature, 392 (1998), pp. 75–78.
[15] N. Ichinose, K. Aihara, and K. Judd, *Extending the concept of isochrons from oscillatory to excitable systems for modeling an excitable neuron*, Internat. J. Bifur. Chaos Appl. Sci. Engrg., 8 (1998), pp. 2375–2385.
[16] A. H. Janardhan, W. Li, V. V. Fedorov, M. Yeung, M. J. Wallendorf, and R. B. Schuessler, and I. R. Efimov, *A novel low-energy electrotherapy that terminates ventricular tachycardia with lower energy than a biphasic shock when antitachycardia pacing fails*, J. Amer. College Cardiology, 60 (2012), pp. 2393–2398.
[17] D. Kirk, *Optimal Control Theory*, Dover, Mineola, NY, 1998.
[18] R. W. Koster, P. Dorian, F. W. Chapman, P. W. Schmitt, S. G. O'Grady, and R. G. Walker, *A randomized trial comparing monophasic and biphasic waveform shocks for external cardioversion of atrial fibrillation*, Amer. Heart J., 147 (2004), pp. e1–e7.
[19] K. Kuck, R. Cappato, J. Siebels, and R. Ruppel, *Randomized comparison of antiarrhythmic drug therapy with implantable defibrillators in patients resuscitated from cardiac arrest: The cardiac arrest study Hamburg*, Circulation, 102 (2000), pp. 748–754.
[20] P. Kudenchuk, L. Cobb, M. Copass, R. Cummins, A. Doherty, C. Fahrenbruch, A. Hallstrom, W. Murray, M. Olsufka, and T. Walshl, *Amiodarone for resuscitation after out-of-hospital cardiac arrest due to ventricular fibrillation*, New England J. Medicine, 341 (1999), pp. 871–878.
[21] W. Li, A. H. Janardhan, V. V. Fedorov, Q. Sha, R. B. Schuessler, and I. R. Efimov, *Low-energy multistage atrial defibrillation therapy terminates atrial fibrillation with less energy than a single shock*, Circulation Arrhythmia Electrophysiol., 4 (2011), pp. 917–925.
[22] D. Lloyd-Jones, R. Adams, T. Brown, M Carnethon, S. Dai, G. De Simone, T. Ferguson, E. Ford, K. Furie, C. Gillespie, A. Go, K. Greenland, N. Haase, S. Hailpern, P. Ho, V. Howard, B. Kisselia, S. Kittner, D. Lackland, L. Lisabeth, A. Marelli, M. McDermott, J. Meigs, D. Mozaffarian, M. Mussolino, G. Nichol, V. Roger, W. Rosamond, R. Sacco, P. Sorlie, R. Stafford, T. Thorn, S. Wasserthiel-Smoller, N. Wong, and J. Wylie-Rossett, *Heart disease and stroke statistics*, Circulation, 121 (2009), pp. e46–e215.
[23] S. Luther, F. Fenton, B. Kornreich, A. Squires, P. Bittihn, D. Hornung, M. Zabel, J. Flanders, A. Gladuli, L. Campoy, E. Cherry, B. Luther, G. Hasenfuss, V. Krinsky, A. Pumir, R. Gilmour, Jr., and E. Bodenschatz, *Low-energy control of electrical turbulence in the heart*, Nature, 475 (2011), pp. 235–241.
[24] A. Mahajan, Y. Shiferaw, D. Sato, A. Baher, R. Olcese, L. Xie, M. Yang, P. Chen, J. G. Restrepo, A. Karma, A. Garfinkel, Z. Qu, and J. N. Weiss, *A rabbit ventricular action potential model replicating cardiac dynamics at rapid heart rates*, Biophys. J., 94 (2008), pp. 392–410.
[25] A. Mauroy, I. Mezic, and J. Moehlis, *Isostables, isochrons, and Koopman spectrum for the action-angle representation of stable fixed point dynamics*, Phys. D, 261 (2013), pp. 19–30.
[26] I. Mitchell, *A Toolbox of Level Set Methods*, Tech. Report TR-2007-11, University of British Columbia,

Vancouver BC, 2007. Available online from http://www.cs.ubs.ca/~mitchell/ToolboxLS/.
[27] A. Nabi, M. Mirzadeh, F. Gibou, and J. Moehlis, *Minimum energy desynchronizing control for coupled neurons*, J. Comput. Neurosci., 34 (2013), pp. 259–271.
[28] J. M. Pastore, S. D. Girouard, K. R. Laurita, F. G. Akar, and D. S. Rosenbaum, *Mechanism linking t-wave alternans to the genesis of cardiac fibrillation*, Circulation, 99 (1999), pp. 1385–1394.
[29] L. Pontryagin, K. N. Trirogoff, and L. Neustadt, *The Mathematical Theory of Optimal Processes*, Wiley, New York, 1962.
[30] W. Press, S. Teukolsky, W. Vetterling, and B. Flannery, *Numerical Recipes: The Art of Scientific Computing*, 3rd ed., Cambridge University Press, New York, 2007.
[31] Z. Qu, A. Garfinkel, P. Chen, and J. N. Weiss, *Mechanisms of discordant alternans and induction of reentry in simulated cardiac tissue*, Circulation, 102 (2000), pp. 1664–1670.
[32] A. Rabinovitch and I. Rogachevskii, *Threshold, excitability and isochrones in the Bonhoeffervan der Pol system*, Chaos, 9 (1999), pp. 880–886.
[33] W. J. Rappel, F. Fenton, and A. Karma, *Spatiotemporal control of wave instabilities in cardiac tissue*, Phys. Rev. Lett., 83 (1999), pp. 456–459.
[34] J. Rogers and A. McCulloch, *A collocation-Galerkin finite element model of cardiac action potential propagation*, IEEE Trans. Biomed. Engrg., 41 (1994), pp. 743–757.
[35] D. S. Rosenbaum, L. E. Jackson, J. M. Smith, H. Garan, J. N. Ruskin, and R. J. Cohen, *Electrical alternans and vulnerability to ventricular arrhythmias*, New England J. Medicine, 330 (1994), pp. 235–241.
[36] S. Sinha, A. Pande, and R. Pandit, *Defibrillation via the elimination of spiral turbulence in a model for ventricular fibrillation*, Phys. Rev. Lett., 86 (2001), pp. 3678–3681.
[37] N. Trayanova, *Concepts of ventricular defibrillation*, Philos. Trans. R. Soc. Lond. Ser. A Math. Phys. Eng. Sci., 359 (2001), pp. 1327–1337.
[38] K. H. W. J. Ten Tusscher and A. V. Panfilov, *Cell model for efficient simulation of wave propagation in human ventricular tissue under normal and pathological conditions*, Phys. Med. Biol., 51 (2006), pp. 6141–6156.
[39] G. Walcott, C. Killingsworth, and R. Ideker, *Do clinically relevant transthoracic defibrillation energies cause myocardial damage and dysfunction?*, Resuscitation, 59 (2003), pp. 59–70.
[40] J. N. Weiss, A. Karma, Y. Shiferaw, P. Chen, A. Garfinkel, and Z. Qu, *From pulsus to pulseless: The saga of cardiac alternans*, Circulation Res., 98 (2006), pp. 1244–1253.
[41] A. Winfree, *The Geometry of Biological Time*, Springer, New York, 2001.
[42] H. Zhang, B. Hu, and G. Hu, *Suppression of spiral waves and spatiotemporal chaos by generating target waves in excitable media*, Phys. Rev. E, 68 (2003), 026134.